Biophysical Reports

LETTER

Chromatin as self-returning walks: From population to single cell and back

Anne R. Shim,[1,2] Kai Huang,[3,*] Vadim Backman,[1,2] and Igal Szleifer[1,2,4,*]

[1]Department of Biomedical Engineering, Northwestern University, Evanston, Illinois; [2]Chemistry of Life Processes Institute, Northwestern University, Evanston, Illinois; [3]Shenzhen Bay Laboratory, Shenzhen, Guangdong Province, P. R. China; and [4]Department of Chemistry, Northwestern University, Evanston, Illinois

ABSTRACT With a growing understanding of the chromatin structure, many efforts remain focused on bridging the gap between what is suggested by population-averaged data and what is visualized for single cells. A popular approach to traversing these scales is to fit a polymer model to Hi-C contact data. However, Hi-C is an average of millions to billions of cells, and each cell may not contain all population-averaged contacts. Therefore, we employ a novel approach of summing individual chromosome trajectories—determined by our Self-Returning Random Walk model—to create populations of cells. We allow single cells to consist of disparate structures and reproduce a variety of experimentally relevant contact maps. We show that the amount of shared topology between cells, and their mechanism of formation, changes the population-averaged structure. Therefore, we present a modeling technique that, with few constraints and little oversight, can be used to understand which single-cell chromatin structures underlie population-averaged behavior.

WHY IT MATTERS In the last decade, many efforts have focused on understanding how chromatin is folded into the nucleus. In large part, this understanding has only been achieved through the invention of novel technologies. While some of these technologies are focused on visualizing chromatin in single cells, much of our understanding has come from techniques which require population averaging. As it is difficult to correlate what is learned at both scales, a large thrust of research is now focused on bridging the gap between what is suggested by population-averaged data and what is visualized for single cells. As there are currently no experimental techniques or analyses that can do so, it is incumbent on models, such as ours, to provide this bridge.

The last decade has witnessed a rapid transformation in our understanding of the chromatin structure. Our burgeoning understanding parallels previously inconceivable technologies, which can be generally categorized as either 1) single-cell imaging of the chromatin structure or 2) population-averaged or bulk data of chromatin contacts or protein accessibility. Advances in imaging include multicolored fluorescent tagging of chromatin, both fluorescent in situ hybridization (FISH) (1–5) and CRISPR (6–11) based, as well as higher-resolution electron microscopy techniques such as ChromEMT (12). Unlike these direct visualization techniques, sequencing-based techniques infer the higher-order structure of chromatin based on the statistics of dissected genomic contacts collected from a large ensemble of cells. With this approach, high-throughput chromosome conformation capture (Hi-C) was the first technique to describe compartments and domains smaller than chromosome territories (10–100 Mb), which are formed through fractal-like (self-similar) folding of the underlying chromatin (13). Even with these great technological advances, one of the most significant questions that remains is how much of the population-averaged structure (determined by Hi-C and other such methods) translates to individual cells. This question is not easily answered, as several studies have detailed a well-known paradox in which loci with frequent Hi-C contacts have been less proximal in space (measured with FISH) than loci with less frequent Hi-C contact (14). In addition, natural variation between cells blurs our understanding of domain localization at the population level (15,16), and domains currently cannot be distinguished with single-cell Hi-C, as the contact maps are too sparse

Submitted August 4, 2021, and accepted for publication December 8, 2021.

*Correspondence: huangkai@szbl.ac.cn or igalsz@northwestern.edu

Editor: Dmitrii Makarov.

https://doi.org/10.1016/j.bpr.2021.100042

(17–19). As single-cell Hi-C and imaging studies are not easily comparable to Hi-C population averages, modeling has intervened to bridge the gap between single-cell and population-averaged chromatin structures; indeed, it is likely only through modeling that these scales can be reconciled (20).

Recently, several efforts have been aimed at understanding how heterogeneous, single-cell structures across a population manifest in population-averaged experimental investigation. Elegant modeling solutions have been aimed at understanding how different experimental modalities could offer conflicting pictures of the chromatin structure (20), integrating several data modalities to allow a convergent understanding of chromatin from multiple viewpoints (21,22) and allowing heterogeneity within averaged structures (23–26). However, despite these efforts, the question is still open for a variety of reasons. One important reason is that these methods are supervised by experimental data, so the structures are inherently biased. Although this is a benefit for reproducing experimentally relevant structures, it still relies on assumptions about the relationship between contact frequencies and how these population-averaged frequencies translate to individual structures. Furthermore, the studies which investigate the role of heterogeneity in the chromatin structure start with the averaged structure and then allow heterogeneity to understand to what extent heterogeneity causes the population-averaged analysis to be altered significantly. While this is integral to our understanding of the chromatin structure, there is still a need for understanding how unbiasedly aggregated structures might appear during population averaging and how heterogeneity within these structures affects population contact maps.

We have recently developed a single-cell, statistical model of chromatin called the Self-Returning Random Walk (SRRW) model, which has excellent agreement with single-cell imaging data; the chromatin density distribution and mass scaling of the modeled chromatin trajectory has excellent agreement with partial wave spectroscopic imaging and ChromSTEM imaging of cells both at homeostasis and while undergoing heat shock (27). This agreement is nontrivial, as our simple model captures the heterogeneity of the chromatin structure, the separation of chromatin into domains, and the fractal-like nature that are experimentally observed and not easily reconciled at the single-cell level (27). In brief, the SRRW models the genome by coarse-graining 2-kb of DNA (∼10 nucleosomes) into steps of variable step sizes, which allows the steps to represent the conformational freedom of a 10-nm fiber at kilobase level (27). Each step size (U_1) is determined from a power-law distribution $P_{\text{jump}}(U_1 > u) = u^{-(\alpha+1)}$, where $u = 1$ restricts the smallest step size in reduced units to be ∼30 nm. α is the universal folding parameter, which not only determines the distribution of step sizes but also which determines the amount of stochastic, self-returning events that occur within the chromatin trajectory and which we introduce to capture the frequent genomic contacts. Here, returns form loops, or branches, within the structure, although it is important to note that these loops may be transient pairwise interactions and are not exclusively representative of loop domains anchored by architectural proteins. The return probability decays with the length of the current step size (U_0), also by a power law: $P_{\text{return}}(U_0) = \frac{U_0^{-\alpha}}{\alpha}$. Intrinsically, large steps have a lower probability of returning than small steps, and smaller α (close to 1) causes a higher return frequency and therefore a higher degree of compaction than larger α. Each SRRW "trajectory" is therefore a sequence of jumps and returns, each of which has a unique step size and orientation in space (orientations are randomly generated). The overall architecture of an SRRW trajectory is a string of random trees (linear stretches of the chromatin with a high degree of returning), which are separated from other trees by unreturned, long jumps called backbone segments, and are organized in a highly nested and hierarchical fashion, as seen in imaging studies (3,28,29). As such, the SRRW model has suggested that single-cell chromatin is more structured and topologically complicated than previously thought, with more higher-order genomic interactions (beyond pairwise contacts) than other models, but which is supported by a growing abundance of experimental evidence (28,29). As previously we performed an analysis of the impact of α on the hierarchical structure predicted by the SRRW model, and $\alpha = 1.15$ was shown to be most similar to interphase chromatin under homeostatic conditions (27), we will use $\alpha = 1.15$ for the remainder of the results in this paper unless stated otherwise.

As the SRRW model has been shown to have excellent agreement with single-cell imaging studies, the logical next step is to use the SRRW model to build a population cell by cell or trajectory by trajectory. The first question that must be answered when constructing a population is: how many single trajectories make up a "population"? Experimental populations contain millions to billions of cells to increase the map resolution (the smallest locus size such that 80% of loci have at least 1000 contacts) (30). Alternatively, our SRRW model achieves a 6-kb map resolution with only 50 conformations. Furthermore, because the SRRW is a statistical model, there is no advantage to simulating millions of cells, as the statistics of the contact map are the same with 1000 cells as they are with 5000 cells (Fig. S1). Therefore, all population averages herein contain 1000 "single-cell" conformations, with which the SRRW model has statistics similar to

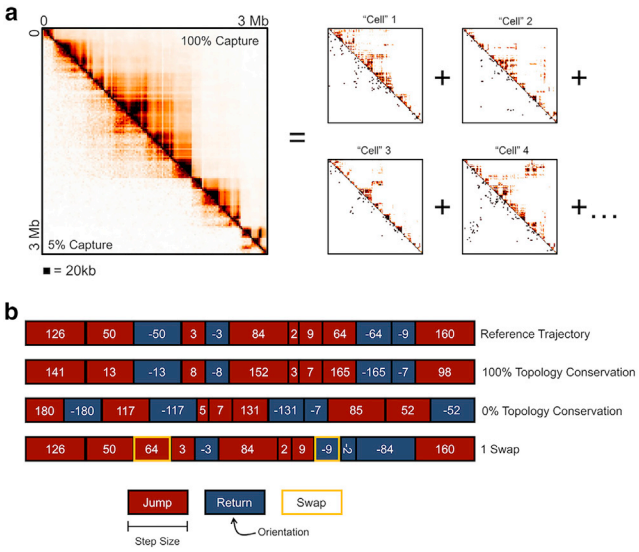

FIGURE 1 Constructing a population of cells from individual SRRW trajectories. (*a*) A contact map for a population of 1000 individual trajectories with 98% shared topology. As seen in the single "cell" conformations, even 2% alteration in topology can lead to many different structures. All contact maps are shown with 100% capture rate (*top right*), which displays every contact in the entire conformation. However, a 5% capture rate of contacts creates both single-cell maps and population-averaged map that are more similar to experimental data. (*b*) Workflow for creating a population from individual SRRW trajectories. We start with a reference trajectory. For 100% topology conservation, the sequence of jumps (*red blocks*), returns (*blue blocks*), and their step sizes (the lengths of the blocks) is the same, but the angles of the steps are newly generated (written within the blocks). Biologically, this would be the same chromatin structure, rotated differently in space. For 0% topology conservation, all features are newly generated for each trajectory. In this case, any shared topology is due to random chance. For intermediate topology conservations, we impose variation by swapping one randomly selected jump and one randomly selected return multiple times to reach the level of topology conservation specified. These swaps either cause a new pairwise interaction (jump to return) or eliminate a pairwise interaction (return to jump).

experimental data with millions of cells and a 6-kb map resolution. We are able to achieve a 6-kb map resolution with so few cells in large part because, as a computational method, we capture all contacts between all loci in the folded structure. Because of this, our contact maps for both single-cell SRRW conformations and population-averaged conformations look more structured than seen experimentally (Fig. 1 *a*, *upper left of contact maps*). However, reducing the capture rate such that only 5% of the contacts in the conformation are recorded causes the contact maps to look very similar to currently available Hi-C data (Fig. 1 *a*, *bottom right of contact maps*). This suggests that the experimental capture rate is not high, possibly due to known experimental limitations, such as sequencing mismatch or the inability to detect interactions above the level of only pairwise interactions. However, although there is mounting evidence from imaging-based studies that the genome is highly hierarchical (3,28,29), and therefore, as we predict, the underlying structures may be much more structured than currently hypothesized, we currently have no way to estimate what capture rate is expected experimentally. Therefore, it is incumbent upon models, such as ours, to perform a computational investigation in order to gain insight into what improvements might be necessary in experimental technologies.

Our population averages are created by averaging the contact maps of 1000 individual SRRW trajectories. As described previously (27), each individual SRRW trajectory is dependent on a universal folding parameter, α. Therefore, we begin by investigating how changing α affects the population-level domains folded by the SRRW model (Fig. 2 *a*). These domains are flanked on either side by a random walk boundary polymer to compare the SRRW domain against a random walk polymer. To fold these domains, we introduce a constraint, the "stop" constraint, whereby we do not allow the domain to fold backward into a previously folded stretch of chromatin. In this case, the stop constraint prevents the domain from returning to the random walk boundary. *In vivo*, this constraint could be imposed by architectural proteins, such as CCCTC-binding factors (CTCF), which demarcate the boundary of domains. This stop constraint causes a buildup of steps at the boundary of the domain such that the stripe feature is created, which was previously thought to only be possible by the attenuation of "loops in the making" at a loop domain (Fig. 2 *a*, *arrow*). This stripe, and the domain itself, disappears as α is raised, indicating that large α values cause domains to fold in a random walk-like fashion, therefore causing the domain to be averaged out. Herein, the remainder of the individual trajectories which comprise our populations are folded with $\alpha = 1.15$, which are far from random walk folding.

The second question that must be answered when constructing a population is: how much variability exists within the population? While natural variation is expected, as structure dictates function it is unlikely that cells are completely uncorrelated. Therefore, we introduce a parameter that we call the "topology conservation," which determines the degree of correlation between cells in a population. Here, topology means the sequence of jumps and returns that create the structure but does not include the orientation of the steps. If we examine a population wherein all cells have the same topology (100% topology conservation), each cell will have the same sequence of jumps, returns, and step sizes, but the orientation (angles) of these steps would be varied cell to cell (Fig. 1 *b*). Biologically, this would correspond to a population wherein each cell has the same sequence of domains, loops, and so forth, but

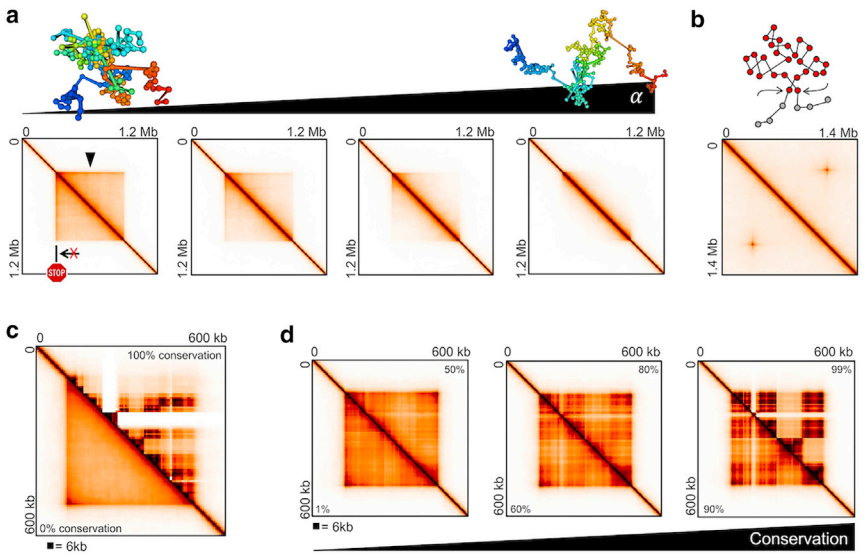

FIGURE 2 α and topology conservation affect population-averaged domains. (*a*) For single domains (600 kb) flanked by a boundary region folded by random walks (300 kb each), increasing α causes the domain to approach the behavior of the random walk boundary regions. These domains are population averages of 1000 independently generated conformations (0% topology conservation) of the same size and α. (*b*) To create loop domains, we introduce the cutoff criterion. This criterion causes the intense bright spot that demarcates the edge of domains. However, the cutoff criterion does not form a domain. To create a loop domain, therefore, both the stop criterion and the cutoff criterion must be applied. (*c*) 100% topology conservation between single cells within the population causes the population-averaged contact map to obscure the corner bright spot (*upper left*). Conversely, the corner bright spot is prevalent if there is no conservation of the inner structure of the domain between the cells within a population (*lower right*). (*d*) Therefore, there must be some continuum for which some topology can be preserved within a population while still allowing the visualization of the corner bright spot. Low topology conservation, less than 50%, allows the corner bright spot to be easily distinguished (*left*). With mid-ranged topology conservation, 60–80%, the corner peak is still visible, but is less distinct from the contacts of the inner structure and may not be distinguished by loop-calling algorithms. High topology conservation, over 90%, causes the entire domain to look highly structured and in contact.

these structures are rotated differently in each cell due to natural variation. Conversely, a population wherein no cells have conserved topology (0% topology conservation) would correspond to a population wherein each cell has a newly generated sequence of jumps, returns, step sizes, and orientations (Fig. 1 *b*). Biologically, this would correspond to a chromatin structure whereby no domains, domain boundaries, or folded structures are the same in all cells, and any shared topology is due to random chance. To create our populations with intermediate topology conservation, we begin with one reference conformation and introduce variation at random. The variation imposed consists of swapping one jump and one return (Fig. 1 *b*). Biologically, a swap from a jump to a return would correspond to a locus creating a new pairwise interaction (due to either looping or clustering), whereas a swap from a return to a jump would dissolve a pairwise interaction. For example, Fig. 1 *a* is a population with 98% topology conservation. Therefore, 2% of each individual conformation is randomly selected for variation. Sometimes, this small variation does not lead to a large change in structure (Fig. 1 *b*, "*Cell" 1* and "*Cell" 2*), while other times even a 2% change in conformation can lead to widespread changes in the existing structures. Importantly, this underscores the difficulty of studying variation within populations. In Fig. 1, only 2% of the linear topology varies cell to cell; however, the way that alterations to the linear chain manifests into three-dimensional structures can be largely altered.

Naturally, this raises the question: how much topology conservation is expected for a population of cells *in vivo*? Domains should not be completely uncorrelated; however, natural function should cause variation in structure from cell to cell. Therefore, experimental populations must exist somewhere on the continuum between 0% topology conservation (Fig. 2 *c*, *bottom left*) and 100% topology conservation (Fig. 2 *c*, *top right*). As we currently do not have any experimental data to suggest where populations fall on this spectrum, we took the approach of determining how much variation replicates experimental contact maps. For this study, we examine loop domains, as they have a clear classification criterion that the corner peak must be at least twice as intense as the average of the rest of the domain. We create loop domains by imposing a new criterion that domains must begin and end within a certain cutoff (150 nm). Interestingly, this cutoff criterion alone does not cause the formation of loop domains (Fig. 2 *b*). Whereas the bright spot that forms at the corner of domains is prevalent due to the cutoff criterion, the intervening contacts are not high enough in intensity compared to the background such that a domain would be identified with topologically associated domain (TAD)-calling algorithms. However, when combining the cutoff criterion with the stop criterion, we find that it is possible to reproduce experimentally similar loop domains, where the boundaries of these loop domains are also folded by the SRRW algorithm (Fig. 2 *c* and *d*). For these population-level loop

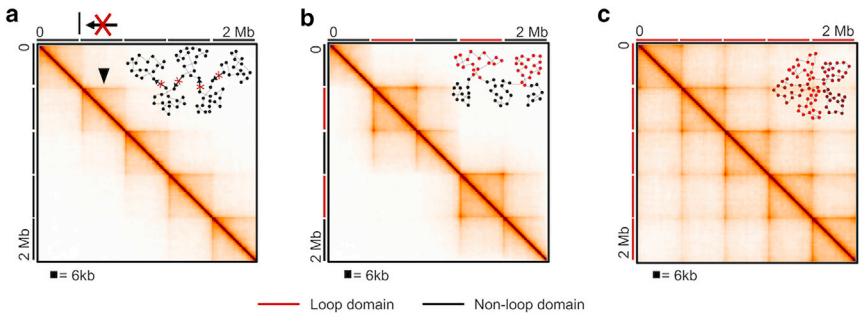

FIGURE 3 Mechanisms of loop and higher-order structure formation. (*a*) Nonloop domains, which are restricted in their returning in one direction, have good isolation and exhibit the stripe feature seen in Hi-C (*arrow*). (*b*) Alternating loop domains with nonloop domains shows good isolation and is different from (*c*) having many consecutive loop domains. Multiple consecutive loop domains is similar to the rosette model, and the contact map created by this rosette is similar to features seen in Hi-C.

domains, it is necessary to have a low degree of conservation to distinguish the corner peak of the loop domains (Fig. 2 *d*). Although the corner peak does not increase in intensity as conservation is decreased, it does increase in contrast as conservation is decreased. Therefore, it is likely that population-averaged loop domains are more dissimilar than they are similar, with shared topology in the range of 0–50%.

Thus far, we have considered how altering the constraints and properties of chromatin folding changes the manifestation of single domains on population-averaged contact maps. It is hypothesized that domains make up the majority of chromatin's higher-order structure. Therefore, we now investigate how adjacent domains manifest on population contact maps. We begin with five adjacent domains with no cutoff criterion and no topology conservation (Fig. 3 *a*). We create these domains separately, folding five 400-kb trajectories and appending each trajectory to the last step of the previous domain. This allows us to impose the stop constraint although, depending on the orientation of each domain, either large or small overlaps between the domains are possible. Note that each domain appears to be identical. This is because there is no topological conservation; therefore, the domains should have the same internal structure on average. Notably, long-range domain isolation can be achieved in these population averages of completely independent conformations just by introducing the stop constraint. Surprisingly, with just this one constraint, we see good isolation between adjacent domains, which had no instruction to avoid overlap.

Next, we impose the cutoff constraint to every other domain (Fig. 3 *b*). However, now we only impose that 50% of the individual conformations must meet the cutoff constraint of 150 nm to allow for the possibility that loop domains are not closed at all times. Experimental data have shown that CTCF has an average residence time of 22–38 min, while cohesin has an average residence time of 20 min (31). In addition, both cohesin and CTCF undergo a 20–30 min search time following detachment from chromatin. Therefore, the probability that a loop domain is closed at any given time is roughly 50%. We fold both the nonloop domains and loop domains separately and, as above, append them to the previous domain. Interestingly, isolation is not as strong between adjacent loop and nonloop domains (Fig. 3 *b*) as between adjacent nonloop domains (Fig. 3 *a*). This supports the hypothesis that some domains are not intentionally created but may be the result of the folding of the chromatin that is in between two loop domains. Additionally, we see a strengthening of the stripes at the boundary of loop domains. This supports two simultaneous mechanisms for the experimentally observed stripe feature. First, as seen with nonloop domains, the stop criterion causes chromatin to accrue at the boundary of domains. Second, because only 50% of loops are closed, the other 50% are in various stages of loop formation, and these “loops in the making” strengthen the intensity of the boundary stripe.

Finally, we investigate the case of adjacent loop domains (Fig. 3 *c*). This contact map not only displays on-diagonal domains with strong corner peaks, but also strong peaks between the corners of all domains. The strength of the peaks, both at the corner of the on-diagonal domains and between the boundaries of these domains, off-diagonal, is dependent on the number of domains within the population that are fully formed. With no broken loops across the population, the corner peaks are much more prominent (Fig. S2). While still distinguishable, these peaks are much less prominent when we impose the cutoff distance constraint for only 50% of the loops (Fig. 3 *c*). Interestingly, this contact map has been observed experimentally (32,33). This contact pattern was hypothesized to indicate the presence of nested subTADs. However, we find that this pattern is more indicative of the hypothesized rosette structure (Fig. 3 *c*, *cartoon*) (34). Here, isolation is not as strong as in the previous cases because domains cannot be as spatially separated while also sharing a single nexus.

Altogether, we present, as far as we know, the first model of population-level chromatin structures that is

created by bottom-up aggregation of single-cell structures, determined by our SRRW model, which has excellent agreement with single-cell experimental chromatin statistics. While other models fit polymer physics to population-level experimental data (35–38), we mimic how populations are formed *in vivo* by aggregating single conformations that are folded 1) with the same degree of conformational freedom as single-cell chromatin, unencumbered by bulky, coarse-grained monomers, and 2) unsupervised by Hi-C data. This allows us to better understand the relationship that single-cell conformations must have with each other to contribute to experimentally observed contact maps, which we are able to reproduce even with this simple, single-parameter model. An important finding of our model is that the amount of shared topology within a population likely is different between loop and nonloop domains. Loop domains have architectural proteins which maintain the domain and therefore need not share this structure across the population. This would not be true for domains without architectural proteins, which would require a high degree of shared topology to be conserved across a population. Therefore, we hypothesize that although nonloop domains likely have little shared topology, nonloop domains are likely highly conserved.

Importantly, unlike other models, the SRRW model does not impose specific folding mechanisms such as loop extrusion (39–42) or phase separation (43,44). However, our model does not exclude the possibility that these, and other, mechanisms are at play. In fact, we believe that the trajectories folded by the SRRW model could be manifested only by employing a combination of nearly all folding mechanisms. For example, loop domains necessitate loop extrusion, whereas many tree domains and subdomains are reminiscent of supercoiling. Even without explicitly imposing a mechanism, we show that chromatin can use local elements to control long-range structure. This asset is shared with the supercoil model: torsion at a local locus can be propagated to a faraway domain.

Of course, the findings presented herein are based on the assumption that interphase chromatin is best represented by $\alpha = 1.15$. While our previous work has demonstrated that SRRW trajectories with $\alpha = 1.15$ have excellent agreement with single-cell experimental analysis of the chromatin structure, it is still likely that α may vary between cells or cell lines (45–48). Indeed, the main limitation of our method is that, as our intention was to analyze how heterogeneities of single-cell chromatin could manifest in population-averaged maps unsupervised by Hi-C data, we currently are unable to compare our results against experimental Hi-C data. This is primarily because, although our population-averaged SRRW contact maps are qualitatively similar to experimental contact maps, the sparsity and heterogeneity of single-cell Hi-C contact maps cannot feasibly be compared to our single-cell SRRW Hi-C maps. However, our study is not completely devoid of experimental consideration. Our SRRW model, in particular with $\alpha = 1.15$, has excellent agreement with experimental analysis of single-cell chromatin, both in terms of DNA mass scaling and in terms of the distribution of chromatin volume concentration (27). As our model is therefore physiologically relevant on the single-cell level, we now use these single-cell structures to determine the degree of similarity that various single-cell chromatin structures would need to have in order to be manifested on population-averaged Hi-C maps. However, now that we have established this framework, in the future we will endeavor to incorporate a data-driven validation with population-level data.

Therefore, we demonstrate a modeling technique that, with few constraints and little oversight, generates heterogeneous structures and allows them to be variable both within and between cells to examine population-averaged chromatin and the way it manifests *in vivo*. By forming populations cell by cell, we are able to compare chromatin structures from population level to single cells and back. In doing so, we find the following: 1) The sparsity of the Hi-C interactome is not due to a lack of structure but rather a lack of ability to detect the structure through current methods. As such, single-cell chromatin is likely more structured than currently hypothesized, but this structure is averaged out by population-averaged study, a conclusion that is being supported by new technologies (28,29,49). 2) Current experimental methods likely have a low capture rate of chromatin contacts. 3) Some structures are more suited to population-averaged study than others, suggesting that a variety of methods employed in tandem might be more useful for understanding the single-cell chromatin structure than any single method alone. Our current understanding of the chromatin structure is built upon novel technologies developed specifically to further our understanding of chromatin *in vivo*, but there is still no experimental technology that could faithfully compare the single-cell chromatin structure with bulk data. Therefore, we hope that our insights in this paper could inspire future efforts to develop technologies to better understand the highly structured, single-cell chromatin, as well as how this structure may or may not be conserved cell to cell.

SUPPORTING MATERIAL

Supporting material can be found online at https://doi.org/10.1016/j.bpr.2021.100042.

AUTHOR CONTRIBUTIONS

A.R.S., K.H., and I.S. conceived the idea for the project. K.H. developed the initial SRRW model and assisted in the translation to population-level analysis. A.R.S. translated the SRRW to the population level, performed analysis, and wrote the manuscript. V.B. provided experimental insight. K.H., I.S., and V.B. edited the manuscript.

DECLARATION OF INTERESTS

The authors declare no competing interests.

ACKNOWLEDGMENTS

We acknowledge funding from the NSF (Biol & Envir Inter of Nano Mat 1833214, EFRI research project EFMA-1830961) and the NIH (National Cancer Institute R01 CA228272 and R01 CA225002).

We acknowledge philanthropic support from Kristin Hudson & Rob Goldman, Ms. Susan Brice & Mr. Jordi Esteve, Mark E. Holliday & Mrs. Ingeborg Schneider, the Christina Carinato Charitable Foundation, and Mr. David Sachs.

REFERENCES

1. Beliveau, B. J., A. N. Boettiger, …, C. T. Wu. 2015. Single-molecule super-resolution imaging of chromosomes and in situ haplotype visualization using Oligopaint FISH probes. *Nat. Commun.* 6:7147.
2. Wang, G., J. R. Moffitt, and X. Zhuang. 2018. Multiplexed imaging of high-density libraries of RNAs with MERFISH and expansion microscopy. *Sci. Rep.* 8:4847.
3. Bintu, B., L. J. Mateo, …, X. Zhuang. 2018. Super-resolution chromatin tracing reveals domains and cooperative interactions in single cells. *Science.* 362:eaau1783.
4. Boettiger, A. N., B. Bogdan, …, X. Zhuang. 2016. Super-resolution imaging reveals distinct chromatin folding for different epigenetic states. *Nature.* 529:418–422.
5. Wang, S., J.-H. Su, …, X. Zhuang. 2016. Spatial organization of chromatin domains and compartments in single chromosomes. *Science.* 353:598–602.
6. Chen, B., L. A. Gilbert, …, B. Huang. 2013. Dynamic imaging of genomic loci in living human cells by an optimized CRISPR/Cas system. *Cell.* 155:1479–1491.
7. Duan, J., G. Lu, …, Y. Zhang. 2014. Genome-wide identification of CRISPR/Cas9 off-targets in human genome. *Cell Res.* 24:1009–1012.
8. Ma, H., A. Naseri, …, T. Pederson. 2015. Multicolor CRISPR labeling of chromosomal loci in human cells. *Proc. Natl. Acad. Sci. U S A.* 112:3002–3007.
9. Ma, H., L. C. Tu, …, T. Pederson. 2016. Multiplexed labeling of genomic loci with dCas9 and engineered sgRNAs using CRISPRainbow. *Nat. Biotechnol.* 34:528–530.
10. Qiu, W., Z. Xu, …, Y. Liu. 2019. Determination of local chromatin interactions using a combined CRISPR and peroxidase APEX2 system. *Nucleic Acids Res.* 47:e52.
11. Xu, H., J. Wang, …, B. Chen. 2020. TriTag: an integrative tool to correlate chromatin dynamics and gene expression in living cells. *Nucleic Acids Res.* 48:13013–13014.
12. Ou, H. D., S. Phan, …, C. C. O'Shea. 2017. ChromEMT: visualizing 3D chromatin structure and compaction in interphase and mitotic cells. *Science.* 357:eaag0025.
13. Lieberman-Aiden, E. L., N. L. van Berkum, …, E. S. Dekker. 2009. Comprehensive mapping of long-range interactions reveals folding principles of the human genome. *Science.* 326:289–293.
14. Fudenberg, G., and M. Imakaev. 2017. FISH-ing for captured contacts: towards reconciling FISH and 3C. *Nat. Methods.* 14:673–678.
15. Eagen, K. P. 2018. Principles of chromosome architecture revealed by Hi-C. *Trends Biochem. Sci.* 43:469–478.
16. Finn, E. H., G. Pegoraro, …, T. Misteli. 2017. Heterogeneity and intrinsic variation in spatial genome organization. *bioRxiv* https://doi.org/10.1101/171801.
17. Kim, H. J., G. G. Yardimci, …, W. S. Noble. 2020. Capturing cell type-specific chromatin compartment patterns by applying topic modeling to single-cell Hi-C data. *PLoS Comput. Biol.* 16:e1008173.
18. Galitsyna, A. A., and M. S. Gelfand. 2021. Single-cell Hi-C data analysis: safety in numbers. *Brief Bioinform.* 22:bbab316.
19. Sekelja, M., J. Paulsen, and P. Collas. 2016. 4D nucleomes in single cells: what can computational modeling reveal about spatial chromatin conformation? *Genome Biol.* 17:54.
20. Shi, G., and D. Thirumalai. 2019. Conformational heterogeneity in human interphase chromosome organization reconciles the FISH and Hi-C paradox. *Nat. Commun.* 10:3894.
21. Benjamin K. Johnson, Jean-Philippe Fortin, Kasper D. Hansen, Hui Shen, Timothy Triche Jr. bioRxiv 2021.05.17.444465; doi: https://doi.org/10.1101/2021.05.17.444465.
22. Pervolarakis, N., Q. H. Nguyen, …, K. Kessenbrock. 2020. Integrated single-cell transcriptomics and chromatin accessibility analysis reveals regulators of mammary epithelial cell identity. *Cell Rep.* 33:108273.
23. Shi, G., and D. Thirumalai. 2021. From Hi-C contact map to three-dimensional organization of interphase human chromosomes. *Phys. Rev. X.* 11:011051.
24. Shi, G., L. Liu, …, D. Thirumalai. 2018. Interphase human chromosome exhibits out of equilibrium glassy dynamics. *Nat. Commun.* 9:3161.
25. Carstens, S., M. Nilges, and M. Habeck. 2020. Bayesian inference of chromatin structure ensembles from population-averaged contact data. *Proc. Natl. Acad. Sci. U S A.* 117:7824–7830.
26. Sun, Q., A. Perez-Rathke, …, J. Liang. 2021. High-resolution single-cell 3D-models of chromatin ensembles during Drosophila embryogenesis. *Nat. Commun.* 12:205.
27. Kai Huang, Y. L., A. R. Shim, …, I. Szleifer. 2020. Physical and data structure of 3D genome. *Sci. Adv.* 6:eaay4055.
28. Allahyar, A., C. Vermeulen, …, W. de Laat. 2018. Enhancer hubs and loop collisions identified from single-allele topologies. *Nat. Genet.* 50:1151–1160.
29. Oudelaar, A. M., J. O. J. Davies, …, J. R. Hughes. 2018. Single-allele chromatin interactions identify regulatory hubs in dynamic compartmentalized domains. *Nat. Genet.* 50:1744–1751.
30. Rao, S. S., M. H. Huntley, …, E. L. Aiden. 2014. A 3D map of the human genome at kilobase resolution reveals principles of chromatin looping. *Cell.* 159:1665–1680.
31. Hansen, A. S., C. Cattoglio, …, R. Tjian. 2018. Recent evidence that TADs and chromatin loops are dynamic structures. *Nucleus.* 9:20–32.
32. Weinreb, C., and B. J. Raphael. 2016. Identification of hierarchical chromatin domains. *Bioinformatics.* 32:1601–1609.
33. Beagan, J. A., and J. E. Phillips-Cremins. 2020. On the existence and functionality of topologically associating domains. *Nat. Genet.* 52:8–16.
34. Knoch, T. A., M. Wachsmuth, …, F. G. Grosveld. 2016. The detailed 3D multi-loop aggregate/rosette chromatin architecture and functional dynamic organization of the human and mouse genomes. *Epigenetics Chromatin.* 9:58.

35. Bendandi, A., S. Dante, …, W. Rocchia. 2020. Chromatin compaction multiscale modeling: a complex synergy between theory, simulation, and experiment. *Front. Mol. Biosci.* 7:15.

36. Bianco, S., D. G. Lupianez, …, M. Nicodemi. 2018. Polymer physics predicts the effects of structural variants on chromatin architecture. *Nat. Genet.* 50:662–667.

37. Onami, S., Y. Taniguchi, …, S. Shinkai. 2020. PHi-C: deciphering Hi-C data into polymer dynamics. *NAR Genom. Bioinform.* 2:lqaa020.

38. Paulsen, J., M. Sekelja, …, P. Collas. 2017. Chrom3D: three-dimensional genome modeling from Hi-C and nuclear lamin-genome contacts. *Genome Biol.* 18:21.

39. Goloborodko, A., J. F. Marko, and L. A. Mirny. 2016. Chromosome compaction by active loop extrusion. *Biophys. J.* 110:2162–2168.

40. Fudenberg, G., M. Imakaev, …, L. A. Mirny. 2016. formation of chromosomal domains by loop extrusion. *Cell Rep.* 15:2038–2049.

41. Fudenberg, G., N. Abdennur, …, L. A. Mirny. 2017. Emerging evidence of chromosome folding by loop extrusion. *Cold Spring Harb. Symp. Quant. Biol.* 82:45–55.

42. Mirny, L. A., and I. Solovei. 2021. Keeping chromatin in the loop(s). *Nat. Rev. Mol. Cell Biol.* 22:439–440.

43. Conte, M., L. Fiorillo, …, M. Nicodemi. 2020. Polymer physics indicates chromatin folding variability across single-cells results from state degeneracy in phase separation. *Nat. Commun.* 11:3289.

44. Narlikar, G. J. 2020. Phase-separation in chromatin organization. *J. Biosci.* 45:5.

45. Chen, C., W. Yu, …, K. Tan. 2019. Spatial genome re-organization between fetal and adult hematopoietic stem cells. *Cell Rep.* 29:4200–4211.e7.

46. Cardozo Gizzi, A. M., D. I. Cattoni, and M. Nollman. 2020. TADs or no TADS: lessons from single-cell imaging of chromosome architecture. *J. Mol. Biol.* 432:682–693.

47. Fraser, J., C. Ferrai, …, M. Nicodemi. 2015. Hierarchical folding and reorganization of chromosomes are linked to transcriptional changes in cellular differentiation. *Mol. Syst. Biol.* 11:852.

48. Shukron, O., V. Piras, …, D. Holcman. 2019. Statistics of chromatin organization during cell differentiation revealed by heterogeneous cross-linked polymers. *Nat. Commun.* 10:2626.

49. Zhang, Y., T. Li, …, B. Ren. 2019. Transcriptionally active HERV-H retrotransposons demarcate topologically associating domains in human pluripotent stem cells. *Nat. Genet.* 51:1380–1388.